Bone Reports 8 (2018) 180–186

Contents lists available at ScienceDirect

Bone Reports

journal homepage: www.elsevier.com/locate/bonr

The reproducibility of measuring trabecular bone parameters using a commercially available high-resolution magnetic resonance imaging approach: A pilot study

Sarah L. West[a,b,*], Chamith S. Rajapakse[c,d], Tammy Rayner[e], Rhiannon Miller[c,d], Michelle A. Slinger[c,d], Greg D. Wells[b,f]

[a] Department of Biology, Trent/Fleming School of Nursing, Trent University, Peterborough, Ontario, Canada
[b] Translational Medicine, The Hospital for Sick Children, Toronto, Ontario, Canada
[c] Department of Radiology, University of Pennsylvania School of Medicine, Philadelphia, PA, USA
[d] Department of Orthopaedic Surgery, University of Pennsylvania School of Medicine, Philadelphia, PA, USA
[e] Radiology, The Hospital for Sick Children, Toronto, Ontario, Canada
[f] Faculty of Kinesiology and Physical Education, University of Toronto, Toronto, Ontario, Canada

ARTICLE INFO

Keywords:
Magnetic resonance imaging
Trabecular microarchitecture
Reproducibility
Bone imaging
Finite element analysis

ABSTRACT

Bone imaging is currently the best non-invasive way to assess changes to bone associated with aging or chronic disease. However, common imaging techniques such as dual energy x-ray absorptiometry are associated with limitations. Magnetic resonance imaging (MRI) is a radiation-free technique that can measure bone microarchitecture. However, published MRI bone assessment protocols use specialized MRI coils and sequences and therefore have limited transferability across institutions. We developed a protocol on a Siemens 3 Tesla MRI machine, using a commercially available coil (Siemens 15 CH knee coil), and manufacturer supplied sequences to acquire images at the tibia. We tested the reproducibility of the FSE and the GE Axial sequences and hypothesized that both would generate reproducible trabecular bone parameters. Eight healthy adults (age 25.5 ± 5.4 years) completed three measurements of each MRI sequence at the tibia. Each of the images was processed for 8 different bone parameters (such as volumetric bone volume fraction). We computed the coefficient of variation (CV) and intraclass correlation coefficients (ICC) to assess reproducibility and reliability. Both sequences resulted in trabecular parameters that were reproducible (CV < 5% for most) and reliable (ICC > 80% for all). Our study is one of the first to report that a commercially available MRI protocol can result in reproducible data, and is significant as MRI may be an accessible method to measure bone microarchitecture in clinical or research environments. This technique requires further testing, including validation and evaluation in other populations.

1. Introduction

Bone loss that is characterized by a decrease in bone mass and a disruption in bone microarchitecture is prevalent in the aging population and in both pediatric and adult cohorts with chronic disease (Cummings et al., 2002; Rodd et al., 2012; Bates et al., 2002; Bouxsein and Seeman, 2009; Legrand et al., 2000; Nickolas et al., 2010; Leonard, 2009; Shanbhogue et al., 2016; Alsufyani et al., 2005; Bhudhikanok et al., 1998; Mostoufi-Moab et al., 2012). Bone imaging techniques are currently the best non-invasive way to assess changes to bone and determine the need for treatment. Bone mineral density (BMD) measured by dual energy X-ray absorptiometry (DXA) is the current standard of care used to evaluate fracture risk (Stone et al., 2003; Miller et al., 1999). However, BMD by DXA has limitations; for example, it produces a 2-dimenstional image of a 3-dimensional structure and it cannot differentiate between cortical and trabecular bone (Bouxsein and Seeman, 2009). This is problematic because areal BMD by DXA does not reflect alterations in bone microarchitecture, which has been shown to independently influence fracture risk (Boutroy et al., 2008; Boutroy et al., 2016).

High-resolution peripheral quantitative computed tomography (HR-pQCT) is an imaging technique that can differentiate between cortical and trabecular bone and can offer insight into structural bone changes including bone microarchitecture and strength. However, HR-pQCT has

* Corresponding author at: Trent University, LHS, D231, 1600 West Bank Drive, Peterborough, Ontario K9L 0G2, Canada.
E-mail addresses: sarahwest@trentu.ca, sarahwest@sickkids.ca (S.L. West).

https://doi.org/10.1016/j.bonr.2018.04.006
Received 2 August 2017; Received in revised form 9 April 2018; Accepted 23 April 2018
Available online 26 April 2018

Table 1
MRI derived trabecular structural and mechanical bone parameters at the tibia.

	Sequence 1 (FSE)					Sequence 2 (GE)				
	Range	Mean	Median CV (%)	IQR of CV	ICC	Range	Mean	Median CV (%)	IQR of CV	ICC
BV/TV (%)	9.03;12.62	10.73	3	4.3	0.88	13.60;17.79	15.53	3.6	2.6	0.84
TbTh (mm)	0.147;0.181	0.156	0.9	2.1	0.85	0.201;0.214	0.206	0.7	0.6	0.95
TbN (mm-1)	0.6;0.77	0.69	2.2	3.2	0.9	0.68;0.83	0.75	3	1.9	0.8
TbS (mm)	1.15;1.52	1.30	2.5	3.4	0.89	0.99;1.28	1.13	3.6	2.3	0.81
TbA (mm^2)	13.65;25.21	17.67	1.5	2.2	0.99	21.18;39.85	27.26	2.1	1.3	0.99
S/C	4.01;7.9	5.78	5.5	6.8	0.94	5.83;12.18	8.90	5.7	4.9	0.93
EI	0.56;1.17	0.8	4.0	5.5	0.98	0.39;0.83	0.6	5.6	4.4	0.92
Stiffness (GPa)	1.61;3.03	2.43	4.4	5.7	0.98	2.26;3.25	2.87	1.8	3.3	0.95

BV/TV: bone volume/total volume; TbTh: trabecular thickness; TbN: trabecular number; TbS: average trabecular spacing; TbA: trabecular area; S/C: surface to curve ratio; EI: erosion index; CV: coefficient of variation; IQR: Interquartile range; ICC: intraclass correlation coefficient.

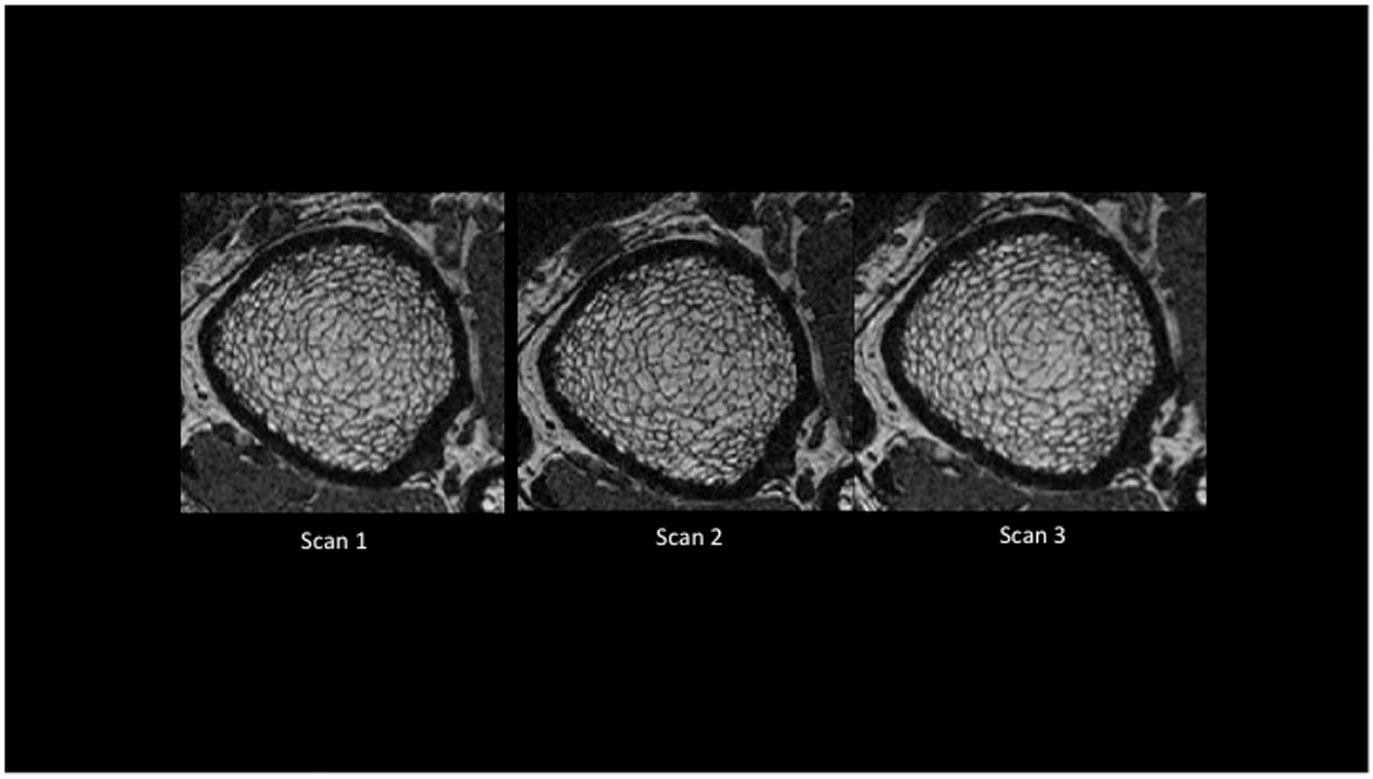

Fig. 1. Repeat images from one participant. Note the visual similarities among all three MRI scans.

limitations. For example, there are a small number of machines currently in use (~20 across Canada and the United States) and this technique is not widely available for clinical or research related evaluations. Furthermore, HR-pQCT measurements are limited to measuring peripheral sites. Recently, modern multidetector row CT (MDCT) has been identified as a reproducible and potentially transferrable trabecular bone imaging technique (Saha et al., 2015; Chen et al., 2017). However, the validity of this technique is unclear (for example, some measures such as trabecular thickness and separation were weakly correlated with gold standard micro-CT-derived values), and although lower than other CT imaging techniques, MDCT exposes individuals to radiation (Chen et al., 2017).

Magnetic resonance imaging (MRI) is associated with many advantages over other bone imaging techniques: 1) it can produce high resolution images that differentiate between cortical and trabecular bone at peripheral skeletal sites (Lam et al., 2011; Wald et al., 2010) and at the hip (Hotca et al., 2015; Chang et al., 2015a); 2) it does not involve ionizing radiation; and 3) machines are available at most major medical institutions. MRI has recently been successful in measuring bone microarchitecture (Lam et al., 2011; Wald et al., 2010; Chang et al., 2015b). However, laboratories that measure bone with MRI often use in-house built MRI coils vs. commercially available coils and in-house developed MRI sequences vs. manufacturer supplied sequences (Lam et al., 2011; Wald et al., 2010). Protocols are therefore not easily transferrable across institutions.

As a first step in addressing this issue, we developed a protocol that uses a commercially available MRI coil and manufacturer supplied sequences to acquire high-resolution images at the tibia. We tested the reproducibility of images produced with two MRI sequences (fast spin echo (FSE) Axial and gradient echo (GE) Axial) by quantifying and comparing trabecular bone parameters. We hypothesized that both MRI sequences would produce images that would generate reproducible trabecular bone microarchitecture outcomes.

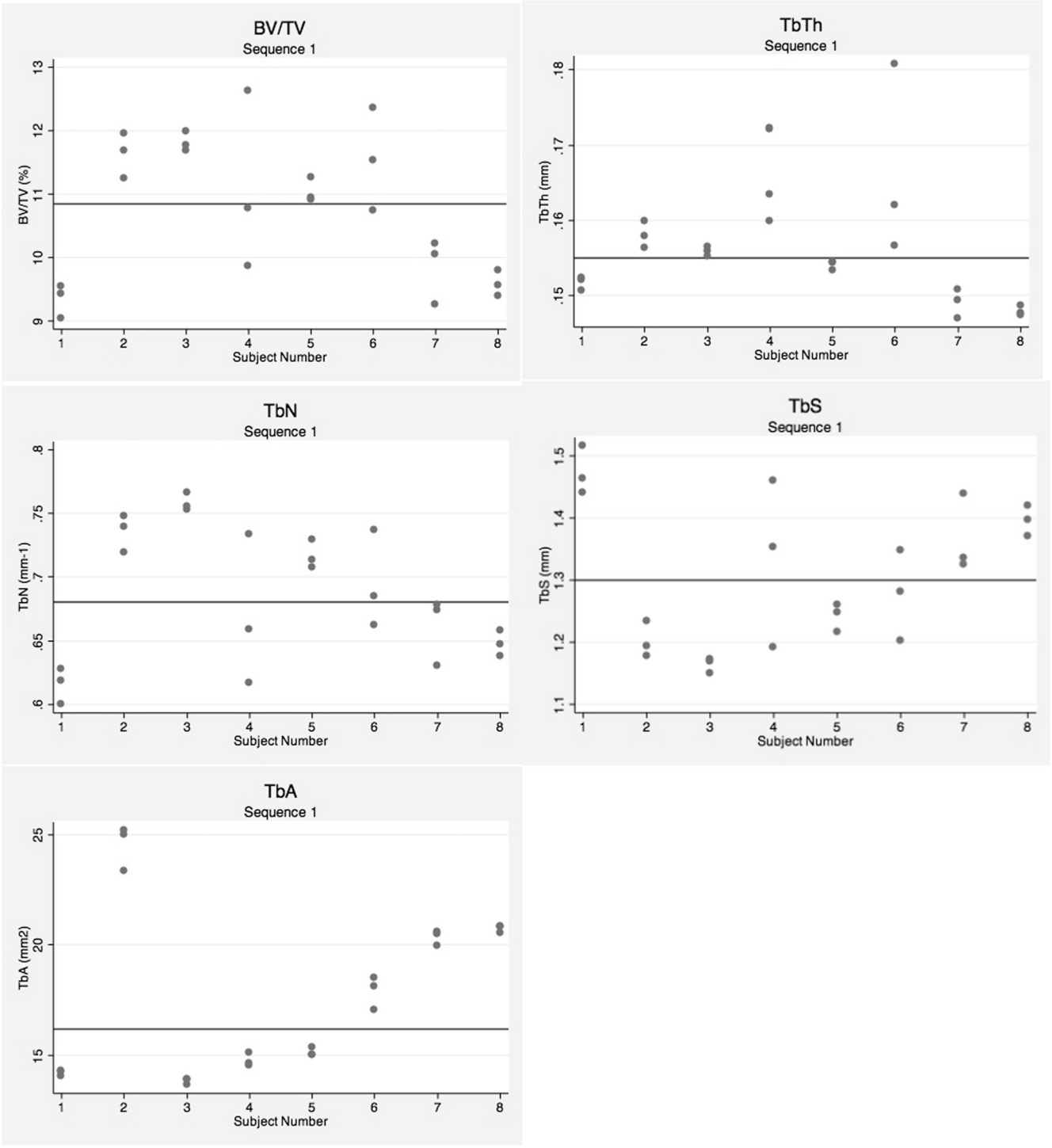

Fig. 2. a. Spread of trabecular structural parameters by subject for sequence 1 (FSE). Dark line indicates median score. b Spread of trabecular structural parameters by subject for sequence 2 (GE). Dark line indicates median score.

2. Materials and methods

2.1. Participants

For this pilot reproducibility study, we recruited healthy adults 18–35 years old (Wald et al., 2010). Participants were required to have a body mass index of < 30 kg/m^2, and no chronic illnesses including osteoporosis, kidney disease, thyroid disease, or metabolic diseases that may have influenced bone health. We chose to include only healthy young adults in our pilot study so that we could first evaluate the MRI

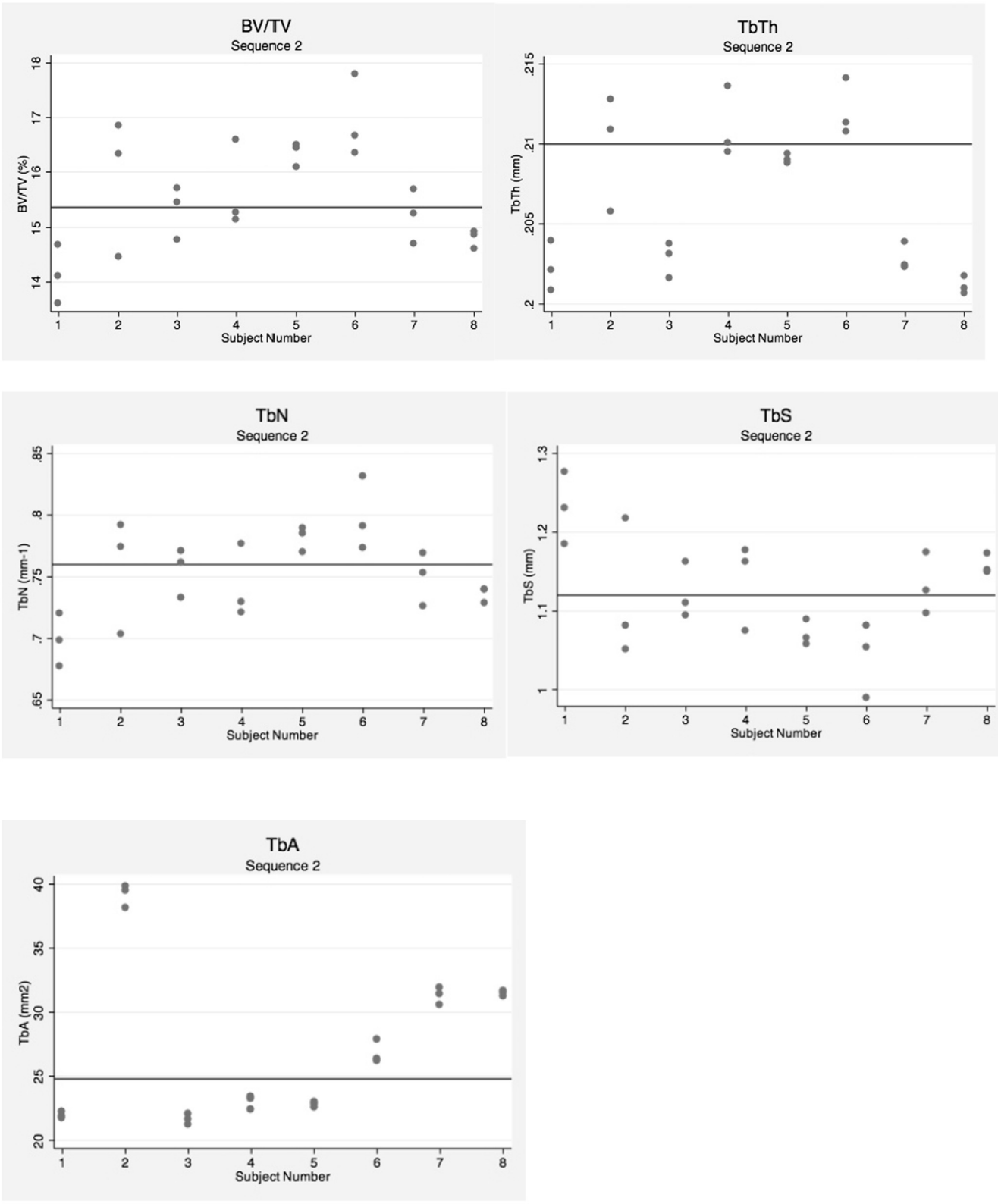

Legend:
BV/TV: bone volume/total volume; TbTh: trabecular thickness; TbN: trabecular number; TbS: average trabecular spacing; TbA: trabecular area

Fig. 2. (*continued*)

Table 2
Comparison of bone parameters (by Wilcoxon Rank-sum test).

Bone parameters	Sequence 1;FSE (median)	Sequence 2;GE (median)	Z	p
BV/TV (%)	10.8	15.4	−5.9	< 0.001
TbTh (mm)	0.155	0.204	−5.9	< 0.001
TbN (mm-1)	0.68	−4.0	0.76	< 0.001
TbS (mm)	1.30	1.12	5.1	< 0.001
TbA (mm^2)	16.20	24.78	−5.2	< 0.001
S/C	5.7	9.1	−5.0	< 0.001
EI	0.8	0.5	4.4	< 0.001
Stiffness (GPa)	2.7	3.05	−3.65	< 0.001

imaging method in a group with no bone health concerns. This study was approved by the SickKids Research Ethics Board (#1000045685), complied with the Declaration of Helsinki, and all participants signed informed consent prior to participating in the study.

2.2. MRI protocol

All testing was conducted at the MRI Research Facility at The Hospital for Sick Children (Toronto, Canada). Upon arrival, the height and weight of the participants was recorded. All imaging was obtained using one MRI machine (Siemens, Tim Trio VB17, 3.0 Tesla) by a single MRI technologist.

Using a tape measure, we measured the length of the tibia from the medial malleolus to the most proximal point of the tibia. We marked 10% of the height of the tibia from the medial malleolus with a piece of removable and MRI safe tape. Participants were asked to lie on the MRI platform feet-first prone position, with their left ankle placed in a Siemens 15 CH knee coil. This particular coil was chosen because of its wide availability on almost all clinical MRI systems. We used foam wedges and Velcro tabs as needed to ensure a snug fit of the lower leg in the coil and to minimize involuntary motion. We ran a localizer sequence (repetition time/echo time [TR/TE]: 7.3/3.6 ms; flip angle: 20; scan time 0:57 s), and then placed the 15 mm sized imaging slab 10 mm proximal to the most proximal tip of the epiphyseal line of the distal tibia, ensuring that the MRI measurements were performed in the metaphysis proximal to the growth plate.

Participants were assessed using FSE Axial (sequence 1) and the GE Axial (sequence 2) sequences. These manufacturer-supplied sequences were chosen as they belong to the same classes of sequence to in-house developed sequences successfully used to measure bone microarchitecture (Wehrli et al., 2001; Wehrli et al., 2004; Magland et al., 2009a; Han et al., 2015; Krug et al., 2009). More specifically, there are two major categories of pulse sequences used for high-resolution MRI of bone microarchitecture. One class of sequences is derived from “gradient echoes”- GE. While sequences derived from this class provide faster acquisitions, images often have line broadening artifacts as a result of successptibility difference between bone and marrow fat manifested as artefactual trabecular bone thickening. The other class of sequences are derived from “spin echoes”—e.g., FSE. These types of sequences are known to reduce susceptibility-induced artifacts but require relatively longer scan times. We therefore chose to evaluate one GE and one FSE sequence in our study.

We ran in succession the FSE Axial (voxel size: 0.2 × 0.2 × 2.0 mm; TR/TE: 659/16 ms; flip angle: 150; 22 slices) and GE Axial sequence (voxel size: 0.3 × 0.3 × 1.0 mm; TR/TE: 13/4.92 ms; flip angle: 40; 14 slices) for a combined scan time of 12 min. The participant was then removed from the MRI machine, asked to stand-up and walk around (on average for 3–5 min), while we removed the 15 CH knee coil and re-set the MRI. The participant returned to the MRI, where he/she was re-landmarked and placed into the MRI and the same sequences were run. Participants completed the MRI protocol 3 times.

2.3. Image processing

After image acquisition, analysis was performed using previously published techniques (Rajapakse et al., 2014; Wehrli et al., 2010). All image processing occurred at the University of Pennsylvania. A region of interest common to the three scans for each participant was isolated and retrospectively registered (Lam et al., 2011; Magland et al., 2009b). Images were converted to bone volume fraction (BVF) images, and structural parameters were derived including: bone volume/total volume (BV/TV; ratio of the segmented bone volume to the total volume of the region of interest), trabecular thickness (TbTh; mean thickness of trabeculae), trabecular number (TbN; the average number of trabeculae per unit length), average trabecular spacing (TbS; mean distance between trabeculae), and trabecular area (TbA; mean area of the Tb compartment) (Lam et al., 2011; Bouxsein et al., 2010; Parfitt et al., 1987). We also determined surface to curve ratio (S/C) and erosion index (EI) (Saha PKC, 1994; Saha PKC, 1996; Saha PKC and Majumder, 1997; Saha PKGBRW, 2000), both of which can be used to describe the trabecular bone network integrity (Lam et al., 2011). Finite element computation was used to evaluate axial stiffness (Magland et al., 2012; Rajapakse et al., 2012). Each of the 8 parameters was calculated for both sequences, for all of the three repeated scans, for each participant. Motion correction was not performed for this study.

2.4. Statistical analyses

Demographic characteristics of the participants were assessed using descriptive statistics. The reproducibility of each bone parameter (by sequence) was assessed by the coefficient of variation (CV). We report median CV to account for non-normalized data distribution. The intraclass correlation coefficient (ICC) was also calculated (Lam et al., 2011) as a measure of statistical reliability. To determine differences in bone parameters by sequence, we performed Wilcoxon rank-sum tests. Statistically significant differences were considered at a $p < 0.05$. Statistical analyses were performed in STATA (11.1, College Station, Texas) and MatLab.

3. Results

3.1. Participants

Nine participants ($n = 5$ female, $n = 4$ male) signed consent to participate. One female participant had extreme motion artifact while in the MRI scanner (regardless of any effort to secure her lower leg or to audibly explain to refrain from moving). As a result, incomplete data was collected and she was excluded from the data analyses. Therefore, all data presented in this manuscript is from n = 4 females and n = 4 males. The mean age of participants was 25.5 ± 5.4 years (female: 25 ± 2.9 years; male: 26 ± 7.6 years), and the mean body mass index (BMI) was 23 ± 3.2 kg/m^2 (female: 21.7 ± 2.9 kg/m^2; male: 24.4 ± 3.2 kg/m^2). Five participants were Caucasian, two participants were Asian, and one was South Asian. The average length of the tibia of the female participants was 37.95 ± 0.07 cm, and the average length of the tibia of male participants was 43.29 ± 0.4 cm.

3.2. MRI data

3.2.1. Reproducibility

A total of 48 scans were analyzed for MRI parameters ([8 participants * 2 sequences] * 3 trials; Table 1). Fig. 1 depicts serial images from one participant that visually demonstrates the similarity of the site imaged for parameter assessment, while Fig. 2 shows the relative spread of trabecular structural parameters, by subject. Reproducibility was generally acceptable for all bone parameters (most variables had a median CV < 5%). One variable, S/C, had a CV above 5% (CV = 5.5%) for sequence 1, and S/C and EI had CVs above 5% for sequence 2

(CV = 5.7 and 5.5%, respectively). ICCs were > 0.80, indicating good agreement among the three measurement trials for all variables across the two sequences (Landis and Koch, 1977).

3.2.2. Bone parameter comparison

We examined the differences in each of the bone parameters, between the two sequences (Table 2). A Wilcoxon rank-sum test indicated that the median values for BV/TV, TbTh, TbN, TbA, and stiffness were all lower when produced using sequence 1 vs. sequence 2 ($p < 0.001$ for all). Conversely measurements of trabecular bone network integrity (S/C and EI) and TbS values were higher when produced using sequence 1 vs. sequence 2 ($p < 0.001$ for all).

4. Discussion

We developed and tested the reproducibility of two MRI protocols using a commercially available coil and manufacturer supplied sequences to acquire high-resolution images at the distal tibia. The images we obtained (Fig. 1) were successfully analyzed for multiple trabecular parameters by previously validated methods (Wald et al., 2010; Rajapakse et al., 2014; Wehrli et al., 2010). Overall, our MRI imaging protocol resulted in reproducible trabecular parameters (median CVs < 6% for all parameters for both sequences). Reliability was strong as well, with all parameter ICCs above 0.80 suggesting agreement among the 3 trials (Landis and Koch, 1977). Our results suggest that the images acquired with the Siemens knee coil and both the FSE Axial or GE Axial sequences produce trabecular structural and mechanical results that are reproducible and reliable in healthy adults.

The trabecular parameters we calculated from our images (including BV/TV, TbTh, TbN, TbS, and TbA) most of which are commonly measured by histological analysis of bone biopsy specimens or HR-pQCT. These structural parameters are important to measure as many of them are negatively impacted in individuals with fractures and are associated with increased fracture risk in postmenopausal women (Boutroy et al., 2008; Boutroy et al., 2016). We also calculated bone stiffness using finite element analysis. Lower bone stiffness is indicative of bone abnormalities and may be also be associated with fractures (Haroon et al., 2015). Therefore, the bone parameters assessed in this study are clinically meaningful and can help provide a detailed assessment of bone health.

Our commercially available MRI imaging method is reproducible, much like other techniques that use in-house build coils and sequences (Lam et al., 2011; Wald et al., 2010). For example, Wald et al. investigated the reproducibility and reliability of a MRI trabecular bone imaging technique at the distal tibia in healthy men and women using their in-house built coil and developed sequences (Lam et al., 2011; Wald et al., 2010). They reported excellent reproducibility results with CVs < 5%. Our study is unique because our commercially available MRI imaging protocols, which may be easily transferrable to use on other Siemens 3.0 T MRI machines with a 15-channel knee coil, produce trabecular parameters that are comparably reliable to in-house developed protocols (Wald et al., 2010).

Interestingly, the data from the current study indicates that although both MRI sequences resulted in reproducible images and data, the trabecular parameter values significantly differed between the two sequences tested. For example, the values for BV/TV, TbTh, TbN, and TbA, were all lower when measured with sequence 1 vs. sequence 2 ($p < 0.001$ for all). This finding is consistent with previous data that indicates that trabecular bone imaging by MRI is associated with susceptibility-induced thickening, such that TbTh is often greater when derived from GE images (Techawiboonwong et al., 2005). Indeed, we observed greater TbTh with images obtained by the GE sequence. It is important to note, however, that the purpose of the current pilot study was to test the reproducibility of images produced with the two MRI sequences (FSE and GE) by quantifying and comparing trabecular bone parameters. We did not attempt to examine the validity of our measurements, as we wanted to establish a reproducible protocol prior to conducting a validity study.

Since we report in the current manuscript reproducibility and reliability of our MRI imaging protocol, our next step study will be to examine the validity of our sequences and calculated structural parameters. One method to accomplish this would be to compare the microarchitecture variables obtained by the MRI sequences with those produced by HR-pQCT (the current gold standard for bone microarchitecture imaging). Another important future direction includes testing the reproducibility and validity of our protocol on other MRI machines at other institutions. This will allow us to examine the transferability of our protocol, and whether or not our imaging technique can be easily used at other sites. One consideration would be to develop a phantom that can uniformly evaluate our protocol across sites and MRI machines (by the same and different manufacturers). Finally, future reproducibility and validity studies should also include imaging other sites, such as the radius, since changes to bone microarchitecture at the distal radius are strongly associated with fracture risk (Nagy et al., 2013).

Despite the positive findings of this study, there are several limitations. Our study was a pilot reproducibility study in 8 participants and results should be confirmed in larger populations. Although The International Society for Clinical Densitometry suggests using 15 patients for precision assessments, this guideline is for BMD by DXA testing. Our $n = 8$ is similar to another MRI reproducibility study (Wald et al., 2010) and was determined to be a sufficient number for a primary MRI reproducibility study. The results of the current study cannot be readily extended to multisite setting due to single operator and same-day scanning method used in current study. The participants in the current study were young and healthy; therefore, we do not know how generalizable the technique may be in other populations such as aging individuals with osteoporosis or those with chronic disease affecting bone health; this is another future direction.

As this was a pilot study, we used image-processing algorithms that were previously optimized to work with higher resolution data. Future studies will investigate how those algorithms could be optimized to work best with the images obtainable through generic coils and standard pulse sequences. We did not perform motion correction for this study. Previously established MRI motion correction approaches using navigator echoes (Song and Wehrli, 1999) or auto-focusing (Lin and Song, 2006) could potentially be implemented in conjunction with the product sequences used in this study; this is a future direction. We selected the MRI resolution so that sufficient signal to noise ratio (SNR) could be achieved within a clinically feasible scan time. To further improve the resolution, we would have to scan longer if we are using the same coil. Future studies will investigate the tradeoffs between resolution, SNR, and scan time. We would also like to investigate how the slice thickness in the current protocol may affect the trabecular parameters in our validity study. Finally, processing the images is a time-consuming procedure that is performed by trained individuals; for increased generalizability streamlining the analysis technique is important.

MRI is a powerful tool that has advantages over other bone imaging techniques. We developed and tested the reproducibility and reliability of protocol to acquire MRI images of the tibia using a commercially available coil and standard pulse sequences. Our study is significant as MRI may be an accessible method to measure bone microarchitecture in clinical or research settings that do not have access to specialized personnel to build MRI coils and sequences; however, validity and transferability of our protocol still need to be evaluated.

Funding agency

SickKids Trainee Start Up Fund & The Exercise Medicine Fund at the Hospital for Sick Children.

Conflict of interest

West SL, Rajapakse CR, Rayner T, Miller R, Slinger MA, Wells GD declare that they have no conflict of interest.

Transparency document

The http://dx.doi.org/10.1016/j.bonr.2018.04.006 associated with this article can be found, in online version.

References

Alsufyani, K.A., Ortiz-Alvarez, O., Cabral, D.A., Tucker, L.B., Petty, R.E., Nadel, H., Malleson, P.N., 2005. Bone mineral density in children and adolescents with systemic lupus erythematosus, juvenile dermatomyositis, and systemic vasculitis: relationship to disease duration, cumulative corticosteroid dose, calcium intake, and exercise. J. Rheumatol. 32 (4), 729–733.

Bates, D.W., Black, D.M., Cummings, S.R., 2002. Clinical use of bone densitometry: clinical applications. JAMA 288 (15), 1898–1900.

Bhudhikanok, G.S., Wang, M.C., Marcus, R., Harkins, A., Moss, R.B., Bachrach, L.K., 1998. Bone acquisition and loss in children and adults with cystic fibrosis: a longitudinal study. J. Pediatr. 133 (1), 18–27.

Boutroy, S., Van Rietbergen, B., Sornay-Rendu, E., Munoz, F., Bouxsein, M.L., Delmas, P.D., 2008. Finite element analysis based on in vivo HR-pQCT images of the distal radius is associated with wrist fracture in postmenopausal women. J. Bone Miner. 23 (3), 392–399.

Boutroy, S., Khosla, S., Sornay-Rendu, E., Zanchetta, M.B., McMahon, D.J., Zhang, C.A., Chapurlat, R.D., Zanchetta, J., Stein, E.M., Bogado, C., Majumdar, S., Burghardt, A.J., Shane, E., 2016. Microarchitecture and peripheral BMD are impaired in post-menopausal Caucasian women with fracture independently of Total hip T-score - an international multicenter study. J. Bone Miner. Res. 31 (6), 1158–1166.

Bouxsein, M.L., Seeman, E., 2009. Quantifying the material and structural determinants of bone strength. Best Pract. Res. Clin. Rheumatol. 23 (6), 741–753.

Bouxsein, M.L., Boyd, S.K., Christiansen, B.A., Guldberg, R.E., Jepsen, K.J., Muller, R., 2010. Guidelines for assessment of bone microstructure in rodents using micro-computed tomography. J. Bone Miner. Res. 25 (7), 1468–1486.

Chang, G., Hotca-Cho, A., Rusinek, H., Honig, S., Mikheev, A., Egol, K., Regatte, R.R., Rajapakse, C.S., 2015a. Measurement reproducibility of magnetic resonance imaging-based finite element analysis of proximal femur microarchitecture for in vivo assessment of bone strength. MAGMA 28 (4), 407–412.

Chang, G., Honig, S., Liu, Y., Chen, C., Chu, K.K., Rajapakse, C.S., Egol, K., Xia, D., Saha, P.K., Regatte, R.R., 2015b. 7 tesla MRI of bone microarchitecture discriminates between women without and with fragility fractures who do not differ by bone mineral density. J. Bone Miner. Metab. 33 (3), 285–293.

Chen, C., Zhang, X., Guo, J., Jin, D., Letuchy, E.M., Burns, T.L., Levy, S.M., Hoffman, E.A., Saha, P.K., 2017. Quantitative imaging of peripheral trabecular bone microarchitecture using MDCT. Med. Phys. 45 (1), 236–249.

Cummings, S.R., Bates, D., Black, D.M., 2002. Clinical use of bone densitometry: scientific review. JAMA 288 (15), 1889–1897.

Han, M., Chiba, K., Banerjee, S., Carballido-Gamio, J., Krug, R., 2015. Variable flip angle three-dimensional fast spin-echo sequence combined with outer volume suppression for imaging trabecular bone structure of the proximal femur. J. Magn. Reson. Imaging 41 (5), 1300–1310.

Haroon, N.N., Paterson, J.M., Li, P., Inman, R.D., Haroon, N., 2015. Patients with ankylosing spondylitis have increased cardiovascular and cerebrovascular mortality: a population-based study. Ann. Intern. Med. 163 (6), 409–416.

Hotca, A., Rajapakse, C.S., Cheng, C., Honig, S., Egol, K., Regatte, R.R., Saha, P.K., Chang, G., 2015. In vivo measurement reproducibility of femoral neck microarchitectural parameters derived from 3T MR images. J. Magn. Reson. Imaging 42 (5), 1339–1345.

Krug, R., Stehling, C., Kelley, D.A., Majumdar, S., Link, T.M., 2009. Imaging of the musculoskeletal system in vivo using ultra-high field magnetic resonance at 7 T. Investig. Radiol. 44 (9), 613–618.

Lam, S.C., Wald, M.J., Rajapakse, C.S., Liu, Y., Saha, P.K., Wehrli, F.W., 2011. Performance of the MRI-based virtual bone biopsy in the distal radius: serial reproducibility and reliability of structural and mechanical parameters in women representative of osteoporosis study populations. Bone 49 (4), 895–903.

Landis, J.R., Koch, G.G., 1977. The measurement of observer agreement for categorical data. Biometrics 33 (1), 159–174.

Legrand, E., Chappard, D., Pascaretti, C., Duquenne, M., Krebs, S., Rohmer, V., Basle, M.F., Audran, M., 2000. Trabecular bone microarchitecture, bone mineral density, and vertebral fractures in male osteoporosis. J. Bone Miner. Res. 15 (1), 13–19.

Leonard, M.B., 2009. A structural approach to skeletal fragility in chronic kidney disease. Semin. Nephrol. 29 (2), 133–143.

Lin, W., Song, H.K., 2006. Improved optimization strategies for autofocusing motion compensation in MRI via the analysis of image metric maps. Magn. Reson. Imaging 24 (6), 751–760.

Magland, J.F., Wald, M.J., Wehrli, F.W., 2009a. Spin-echo micro-MRI of trabecular bone using improved 3D fast large-angle spin-echo (FLASE). Magn. Reson. Med. 61 (5), 1114–1121.

Magland, J.F., Jones, C.E., Leonard, M.B., Wehrli, F.W., 2009b. Retrospective 3D registration of trabecular bone MR images for longitudinal studies. J. Magn. Reson. Imaging 29 (1), 118–126.

Magland, J.F., Zhang, N., Rajapakse, C.S., Wehrli, F.W., 2012. Computationally-optimized bone mechanical modeling from high-resolution structural images. PLoS One 7 (4), e35525.

Miller, P.D., Zapalowski, C., Kulak, C.A., Bilezikian, J.P., 1999. Bone densitometry: the best way to detect osteoporosis and to monitor therapy. J. Clin. Endocrinol. Metab. 84 (6), 1867–1871.

Mostoufi-Moab, S., Brodsky, J., Isaacoff, E.J., Tsampalieros, A., Ginsberg, J.P., Zemel, B., Shults, J., Leonard, M.B., 2012. Longitudinal assessment of bone density and structure in childhood survivors of acute lymphoblastic leukemia without cranial radiation. J. Clin. Endocrinol. Metab. 97 (10), 3584–3592.

Nagy, H., Sornay-Rendu, E., Boutroy, S., Vilayphiou, N., Szulc, P., Chapurlat, R., 2013. Impaired trabecular and cortical microarchitecture in daughters of women with osteoporotic fracture: the MODAM study. Osteoporos. Int. 24 (6), 1881–1889.

Nickolas, T.L., Shirazian, S., Shane, E., 2010. High-resolution computed tomography imaging: a virtual bone biopsy. Kidney Int. 77 (11), 1046.

Parfitt, A.M., Drezner, M.K., Glorieux, F.H., Kanis, J.A., Malluche, H., Meunier, P.J., Ott, S.M., Recker, R.R., 1987. Bone histomorphometry: standardization of nomenclature, symbols, and units. J Bone Miner Res 2, 595–610 (Report of the ASBMR Histomorphometry Nomenclature Committee).

Rajapakse, C.S., Leonard, M.B., Bhagat, Y.A., Sun, W., Magland, J.F., Wehrli, F.W., 2012. Micro-MR imaging-based computational biomechanics demonstrates reduction in cortical and trabecular bone strength after renal transplantation. Radiology 262 (3), 912–920.

Rajapakse, C.S., Phillips, E.A., Sun, W., Wald, M.J., Magland, J.F., Snyder, P.J., Wehrli, F.W., 2014. Vertebral deformities and fractures are associated with MRI and pQCT measures obtained at the distal tibia and radius of postmenopausal women. Osteoporos. Int. 25 (3), 973–982.

Rodd, C., Lang, B., Ramsay, T., Alos, N., Huber, A.M., Cabral, D.A., Scuccimarri, R., Miettunen, P.M., Roth, J., Atkinson, S.A., Couch, R., Cummings, E.A., Dent, P.B., Ellsworth, J., Hay, J., Houghton, K., Jurencak, R., Larche, M., LeBlanc, C., Oen, K., Saint-Cyr, C., Stein, R., Stephure, D., Taback, S., Lentle, B., Matzinger, M., Shenouda, N., Moher, D., Rauch, F., Siminoski, K., Ward, L.M., 2012. Canadian steroid-associated osteoporosis in the pediatric population C. Incident vertebral fractures among children with rheumatic disorders 12 months after glucocorticoid initiation: a national observational study. Arthritis Care Res. 64 (1), 122–131.

Saha PKC, B.B., 1994. Detection of 3-D simple points for topology preserving transformations with application to thinning. IEEE Trans. Pattern Anal. Mach. Intell. 16 (10), 1028–1032.

Saha PKC, B.B., 1996. 3D Digital Topology under Binary Transformation with Applications. Comput. Vis. Image Underst. 63 (3), 418–429.

Saha PKC, B.B., Majumder, D.D., 1997. A new shape preserving parallel thinning algorithm for 3D digital images. Pattern Recogn. 30 (12), 1939–1955.

Saha PKGBRW, F.W., 2000. Three-dimensional digital topological characterization of cancellous bone architecture. Int. J. Imaging Syst. Technol. 11 (1), 81–90.

Saha, P.K., Liu, Y., Chen, C., Jin, D., Letuchy, E.M., Xu, Z., Amelon, R.E., Burns, T.L., Torner, J.C., Levy, S.M., Calarge, C.A., 2015. Characterization of trabecular bone plate-rod microarchitecture using multirow detector CT and the tensor scale: algorithms, validation, and applications to pilot human studies. Med. Phys. 42 (9), 5410–5425.

Shanbhogue, V.V., Brixen, K., Hansen, S., 2016. Age- and sex-related changes in bone microarchitecture and estimated strength. A three-year prospective study using HR-pQCT. J. Bone Miner. Res. 31 (8), 1541–1549.

Song, H.K., Wehrli, F.W., 1999. In vivo micro-imaging using alternating navigator echoes with applications to cancellous bone structural analysis. Magn. Reson. Med. 41 (5), 947–953.

Stone, K.L., Seeley, D.G., Lui, L.Y., Cauley, J.A., Ensrud, K., Browner, W.S., Nevitt, M.C., Cummings, S.R., Osteoporotic Fractures Research, G., 2003. BMD at multiple sites and risk of fracture of multiple types: long-term results from the study of osteoporotic fractures. J. Bone Miner. Res. 18 (11), 1947–1954.

Techawiboonwong, A., Song, H.K., Magland, J.F., Saha, P.K., Wehrli, F.W., 2005. Implications of pulse sequence in structural imaging of trabecular bone. J. Magn. Reson. Imaging 22 (5), 647–655.

Wald, M.J., Magland, J.F., Rajapakse, C.S., Wehrli, F.W., 2010. Structural and mechanical parameters of trabecular bone estimated from in vivo high-resolution magnetic resonance images at 3 tesla field strength. J. Magn. Reson. Imaging 31 (5), 1157–1168.

Wehrli, F.W., Gomberg, B.R., Saha, P.K., Song, H.K., Hwang, S.N., Snyder, P.J., 2001. Digital topological analysis of in vivo magnetic resonance microimages of trabecular bone reveals structural implications of osteoporosis. J. Bone Miner. Res. 16 (8), 1520–1531.

Wehrli, F.W., Leonard, M.B., Saha, P.K., Gomberg, B.R., 2004. Quantitative high-resolution magnetic resonance imaging reveals structural implications of renal osteodystrophy on trabecular and cortical bone. J. Magn. Reson. Imaging 20 (1), 83–89.

Wehrli, F.W., Rajapakse, C.S., Magland, J.F., Snyder, P.J., 2010. Mechanical implications of estrogen supplementation in early postmenopausal women. J. Bone Miner. Res. 25 (6), 1406–1414.